Inorg. Chem. **2005**, *44*, 3919–3925

Mixed-Metal Tellurites: Synthesis, Structure, and Characterization of $Na_{1.4}Nb_3Te_{4.9}O_{18}$ and $NaNb_3Te_4O_{16}$

Kang Min Ok and P. Shiv Halasyamani*

Department of Chemistry and Center for Materials Chemistry, 136 Fleming Building, University of Houston, Houston, Texas 77204-5003

Received February 18, 2005

Two new mixed-metal tellurites, $Na_{1.4}Nb_3Te_{4.9}O_{18}$ and $NaNb_3Te_4O_{16}$, have been synthesized by standard solid-state techniques using Na_2CO_3, Nb_2O_5, and TeO_2 as reagents. The structures of $Na_{1.4}Nb_3Te_{4.9}O_{18}$ and $NaNb_3Te_4O_{16}$ were determined by single-crystal X-ray diffraction. Both of the materials exhibit three-dimensional structures composed of NbO_6 octahedra, TeO_4, and TeO_3 polyhedra. The Nb^{5+} and Te^{4+} cations are in asymmetric coordination environments attributable to second-order Jahn–Teller (SOJT) effects. The Nb^{5+} cations undergo an intraoctahedral distortion toward a corner (local C_4 direction), whereas the Te^{4+} cations are in distorted environments owing to their nonbonded electron pair. Infrared and Raman spectroscopy, UV–vis diffuse reflectance spectroscopy, thermogravimetric analysis, and dielectric measurements were also performed on the reported materials. Crystal data: $Na_{1.4}Nb_3Te_{4.9}O_{18}$, monoclinic, space group $C2/m$ (No. 12), with $a = 32.377(5)$ Å, $b = 7.4541(11)$ Å, $c = 6.5649(9)$ Å, $\beta = 95.636(5)°$, $V = 1576.7(4)$ Å^3, and $Z = 4$; $NaNb_3Te_4O_{16}$, monoclinic, space group $P2_1/m$ (No. 11), with $a = 6.6126(13)$ Å, $b = 7.4738(15)$ Å, $c = 14.034(3)$ Å, $\beta = 102.98(3)°$, $V = 675.9(3)$ Å^3, and $Z = 2$.

Introduction

Asymmetric cationic coordination environments in oxide materials are critical to technologically important physical properties such as ferroelectricity, piezoelectricity, pyroelectricity, dielectric behavior, and second-harmonic generation.[1−8] Octahedrally coordinated d^0 transition metals (Ti^{4+}, V^{5+}, Nb^{5+}, Mo^{6+}, etc.) and lone-pair cations (Pb^{2+}, Sb^{3+}, Te^{4+}, I^{5+}, etc.) are often observed in asymmetric coordination environments, attributable to second-order Jahn−Teller (SOJT) effects.[9−15] With the former group, SOJT effects occur when the empty d-orbitals of the metal mix with the filled p-orbitals of the ligands, whereas, with the latter group of cations, a nonbonded electron pair is observed that "pushes" the oxide ligands toward one side of the cation.[16−25] In both instances, an asymmetric coordination environment is observed. With the d^0 transition metals, the cation may distort toward an edge (local C_2 direction, [110]), a face (local C_3 direction, [111]), or a corner (local C_4 direction, [001]), whereas for the lone-pair cations the distortion is toward the

* Author to whom correspondence should be addressed. E-mail: psh@uh.edu. Phone: 713-743-3278. Fax: 713-743-0796.

(1) Jona, F.; Shirane, G. *Ferroelectric Crystals*; Pergamon Press: Oxford, U.K., 1962.
(2) Cady, W. G. *Piezoelectricity; an Introduction to the Theory and Applications of Electromechanical Phenomena in Crystals*; Dover: New York, 1964.
(3) Lang, S. B. *Sourcebook of Pyroelectricity*; Gordon & Breach Science: London, 1974.
(4) Haertling, G. H. In *Electrooptic Ceramics and Devices*; Levinson, L. M., Ed.; Marcel Dekker: New York, 1988; p 371.
(5) Choy, J.-H.; Han, Y.-S.; Kim, J.-T. *J. Mater. Chem.* **1995**, *5*, 65.
(6) Freer, R. *Br. Ceram. Soc. Proc.* **1995**, *55*, 171.
(7) Auciello, O.; Scott, J. F.; Ramesh, R. *Phys. Today* **1998**, *40*, 22.
(8) Macquart, R.; Kennedy, B. J.; Kubota, Y.; Nishibori, E.; Takata, M. *Ferroelectrics* **2000**, *248*, 27.
(9) Opik, U.; Pryce, M. H. L. *Proc. R. Soc. London* **1957**, *A238*, 425.
(10) Bader, R. F. W. *Mol. Phys.* **1960**, *3*, 137.
(11) Bader, R. F. W. *Can. J. Chem.* **1962**, *40*, 1164.
(12) Pearson, R. G. *J. Am. Chem. Soc.* **1969**, *91*, 4947.
(13) Pearson, R. G. *J. Mol. Struct. (THEOCHEM)* **1983**, *103*, 25.
(14) Wheeler, R. A.; Whangbo, M.-H.; Hughbanks, T.; Hoffmann, R.; Burdett, J. K.; Albright, T. A. *J. Am. Chem. Soc.* **1986**, *108*, 2222.
(15) Kunz, M.; Brown, I. D. *J. Solid State Chem.* **1995**, *115*, 395.
(16) Sidgwick, N. V.; Powell, H. M. *Proc. R. Soc. London* **1940**, *A176*, 153.
(17) Gillespie, R. J.; Nyholm, R. S. *Q. Rev., Chem. Soc.* **1957**, *11*, 339.
(18) Orgel, L. *J. Chem. Soc.* **1959**, 3815.
(19) Lefebvre, I.; Lannoo, M.; Allan, G.; Ibanez, A.; Fourcade, J.; Jumas, J. C. *Phys. Rev. Lett.* **1987**, *59*, 2471.
(20) Lefebvre, I.; Szymanski, M. A.; Olivier-Fourcade, J.; Jumas, J. C. *Phys. Rev. B* **1998**, *58*, 1896.
(21) Goodenough, J. B. *Annu. Rev. Mater. Sci.* **1998**, *28*, 1.
(22) Watson, G. W.; Parker, S. C. *J. Phys. Chem. B* **1999**, *103*, 1258.
(23) Watson, G. W.; Parker, S. C.; Kresse, G. *Phys. Rev. B* **1999**, *59*, 8481.
(24) Seshadri, R.; Hill, N. A. *Chem. Mater.* **2001**, *13*, 2892.
(25) Waghmare, U. V.; Spaldin, N. A.; Kandpal, H. C.; Seshadri, R. *Phys. Rev. B* **2003**, *67*, 125111.

10.1021/ic050256b CCC: $30.25
Published on Web 05/04/2005

nonbonded electron pair. These "directional" displacements have been described as primary distortions, whereas secondary distortions are defined as the interaction between the d^0 transition metal octahedron and the lone-pair polyhedron, i.e., lattice distortions.[15,26] With respect to $Nb^{5+}-Te^{4+}-$oxides, few materials have been reported, namely $Te_3Nb_2O_{11}$,[27] $Ba_2Nb_6Te_2O_{21}$,[28] $Nb_2Te_4O_{13}$,[29] $BiNbTe_2O_8$,[30] $Te_4Nb_3O_{15}{\cdot}Cl$,[31] $LaTeNbO_6$,[32] $BaTeNbO_4(PO_4)$,[33] and $Pb_4Te_6Nb_{10}O_{41}$.[34] In all of these materials, NbO_6 octahedra are observed. Of the 20 unique NbO_6 octahedra, 14 contain Nb^{5+} intraoctahedrally distorted toward a corner, i.e., a C_4 distortion. The prevalence of C_4-Nb^{5+} displacements is consistent with our earlier observations.[35] With respect to Te^{4+}, both TeO_3 and TeO_4 polyhedra are observed. In this paper, we report on the synthesis and characterization of two new quaternary oxides, $Na_{1.4}Nb_3Te_{4.9}O_{18}$ and $NaNb_3Te_4O_{16}$. In addition to describing their crystal structures, we discuss primary and secondary distortion concepts as well as the local dipole moments in the NbO_6, TeO_4, and TeO_3 polyhedra.

Experimental Section

Reagents. Na_2CO_3 (Alfa Aesar, 99.5%), Nb_2O_5 (Alfa Aesar, 99%), Na_2TeO_3 (Aldrich, 99%), and TeO_2 (Aldrich, 99%) were used as received.

Synthesis. Crystals of $Na_{1.4}Nb_3Te_{4.9}O_{18}$ were prepared by placing an intimate mixture of Na_2CO_3 (0.106 g, 1.00×10^{-3} mol), Nb_2O_5 (0.266 g, 0.10×10^{-3} mol), and TeO_2 (1.277 g, 8.00×10^{-3} mol) into a platinum crucible that was gradually heated to 760 °C, held for 15 h, and then cooled slowly to 500 °C at 6 °C h^{-1} before being quenched to room temperature. Colorless block-shaped crystals of $Na_{1.4}Nb_3Te_{4.9}O_{18}$ (72% yield based on Nb_2O_5) were recovered with TeO_2 from the crucible. Pure polycrystalline $Na_{1.4}Nb_3Te_{4.9}O_{18}$ was synthesized through standard solid-state techniques. A stoichiometric mixture of Na_2CO_3 (0.225 g, 2.12×10^{-3} mol), Nb_2O_5 (1.208 g, 4.54×10^{-3} mol), and TeO_2 (2.418 g, 14.85×10^{-3} mol) was thoroughly ground and pressed into a pellet. The pellet was heated to 550, 600, and 650 °C for 24 h in air with intermittent regrinding. Powder X-ray diffraction pattern on the resultant white powders indicated the material was single-phase and in agreement with the generated pattern from the single-crystal data (see Supporting Information).

Single crystals of $NaNb_3Te_4O_{16}$ were prepared by transferring a well ground reaction mixture of Na_2TeO_3 (0.111 g, 5.00×10^{-4} mol), Nb_2O_5 (0.399 g, 1.50×10^{-3} mol), and TeO_2 (0.559 g, 3.50×10^{-3} mol) into a platinum crucible. The crucible was heated to 800 °C, held for 15 h, and cooled to 500 °C at 6 °C h^{-1} before being quenched to room temperature. The product contained colorless block-shaped crystals (32% yield based on Nb_2O_5) along with polycrystalline $NaNb_3Te_4O_{16}$, Nb_2O_5, and an unknown material. Several attempts to grow single crystals of $NaNb_3Te_4O_{16}$ with excess TeO_2, either using Na_2TeO_3 or combination of Na_2CO_3 and TeO_2 at 760 °C, produced $Na_{1.4}Nb_3Te_{4.9}O_{18}$ crystals. $NaNb_3Te_4O_{16}$ powder was recovered by using a stoichiometric amount of starting reagents, if the reaction temperature was lower than 800 °C. Pure $NaNb_3Te_4O_{16}$ was obtained by reacting a stoichiometric amount of Na_2TeO_3 (0.222 g, 1.00×10^{-3} mol), Nb_2O_5 (0.798 g, 3.00×10^{-3} mol), and TeO_2 (1.118 g, 7.00×10^{-3} mol). This reaction mixture was ground thoroughly, pressed into a pellet, and heated to 700 °C for 3 days with two intermittent regrindings. The powder X-ray diffraction pattern on the resultant white powder confirmed the material was single-phase and in agreement with the generated X-ray powder pattern from the single-crystal data (see Supporting Information).

Crystallographic Determination. The structures of $Na_{1.4}Nb_3Te_{4.9}O_{18}$ and $NaNb_3Te_4O_{16}$ were determined by standard crystallographic methods. Colorless blocks for $Na_{1.4}Nb_3Te_{4.9}O_{18}$ ($0.06 \times 0.08 \times 0.10$ mm^3) and $NaNb_3Te_4O_{16}$ ($0.04 \times 0.06 \times 0.10$ mm^3) were used for single-crystal measurements. Room-temperature intensity data were collected on a Siemens SMART diffractometer equipped with a 1K CCD area detector using graphite-monochromated Mo Kα radiation. A hemisphere of data was collected using a narrow-frame method with scan widths of 0.30° in ω and an exposure time of 30 s/frame. The first 50 frames were remeasured at the end of the data collection to monitor instrument and crystal stabilities. The maximum correction applied to the intensities was <1%. The data were integrated using the Siemens SAINT program,[36] with the intensities corrected for Lorentz, polarization, air absorption, and absorption attributable to the variation in the path length through the detector faceplate. Ψ-scans were used for the absorption correction on the hemisphere of data. The data were solved and refined using SHELXS-97 and SHELXL-97, respectively.[37,38] All atoms were refined with anisotropic thermal parameters and converged for $I > 2\sigma(I)$. During the course of the refinement for $Na_{1.4}Nb_3Te_{4.9}O_{18}$, we also determined fractional occupancy must occur for two reasons. First, the displacement parameters for Na(1) and Te(1) atoms were relatively higher than those of the other atoms if they were fully occupied. Second, to retain charge balance, Na(1) and Te(1) atoms should not be fully occupied. The most reasonable and structurally sensible model was to refine the occupancies of Na(1) and Te(1). In doing so, partial occupancies of 0.7010(10) and 0.8943(18) were refined for Na(1) and Te(1), respectively (see Supporting Information). All calculations were performed using the WinGX-98 crystallographic software package.[39] Crystallographic data and selected bond distances for $Na_{1.4}Nb_3Te_{4.9}O_{18}$ and $NaNb_3Te_4O_{16}$ are given in Tables 1 and 2, with additional details found in the Supporting Information.

Powder Diffraction. The X-ray powder diffraction data were collected on a Scintag XDS2000 diffractometer at room temperature (Cu Kα radiation, $\theta-\theta$ mode, flat plate geometry) equipped with Peltier germanium solid-state detector in the 2θ range 5−60° with a step size of 0.02° and a step time of 1 s.

Infrared and Raman Spectroscopy. Infrared spectra were recorded on a Matteson FTIR 5000 spectrometer in the 400−4000 cm^{-1} range, with the sample pressed between two KBr pellets.

(26) Welk, M. E.; Norquist, A. J.; Arnold, F. P.; Stern, C. L.; Poeppelmeier, K. R. *Inorg. Chem.* **2002**, *41*, 5119.
(27) Galy, J.; Lindqvist, O. *J. Solid State Chem.* **1979**, *27*, 279.
(28) Muller-Buschbaum, H.; Wedel, B. *Z. Naturforsch.* **1996**, *B51*, 1411.
(29) Blanchandin, S.; Champarnaud-Mesjard, J. C.; Thomas, P.; Frit, B. *J. Alloys Compd.* **2000**, *306*, 175.
(30) Blanchandin, S.; Champarnaud-Mesjard, J. C.; Thomas, P.; Frit, B. *Solid State Sci.* **2000**, *2*, 223.
(31) Ok, K. M.; Halasyamani, P. S. *Inorg. Chem.* **2002**, *41*, 3805.
(32) Ok, K. M.; Zhang, L.; Halasyamani, P. S. *J. Solid State Chem.* **2003**, *175*, 264.
(33) Ok, K. M.; Orzechowski, J.; Halasyamani, P. S. *Inorg. Chem.* **2004**, *43*, 964.
(34) Ok, K. M.; Halasyamani, P. S. *Inorg. Chem.* **2004**, *43*, 4248.
(35) Halasyamani, P. S. *Chem. Mater.* **2004**, *16*, 3586.
(36) *SAINT, version 4.05*: *Program for Area Detector Absorption Correction*; Siemens Analytical X-ray Instruments: Madison, WI, 1995.
(37) Sheldrick, G. M.; *SHELXS-97-A program for automatic solution of crystal structures*; University of Goettingen: Goettingen, Germany, 1997.
(38) Sheldrick, G. M.; *SHELXL-97-A program for crystal structure refinement*; University of Goettingen: Goettingen, Germany, 1997.
(39) Farrugia, L. J. *J. Appl. Crystallogr.* **1999**, *32*, 837.

Table 1. Crystallographic Data for $Na_{1.4}Nb_3Te_{4.9}O_{18}$ and $NaNb_3Te_4O_{16}$

param	$Na_{1.4}Nb_3Te_{4.9}O_{18}$	$NaNb_3Te_4O_{16}$
fw	1224.16	1068.12
space group	*C*2/*m* (No. 12)	$P2_1/m$ (No. 11)
a (Å)	32.377(5)	6.6126(13)
b (Å)	7.4541(11)	7.4738(15)
c (Å)	6.5649(9)	14.034(3)
β (deg)	95.636(5)	102.98(3)
V (Å^3)	1576.7(4)	675.9(3)
Z	4	2
T (°C)	293.0(2)	293.0(2)
λ (Å)	0.710 73	0.710 73
ρ_{calcd} (g cm^{-3})	5.157	5.249
μ (mm^{-1})	11.168	11.087
$R(F)^a$	0.0337	0.0328
$R_w(F_o^2)^b$	0.0836	0.0752

^{a} $R(F) = \Sigma||F_o| - |F_c||/\Sigma|F_o|$. ^{b} $R_w(F_o^2) = [\Sigma w(F_o^2 - F_c^2)^2/\Sigma w(F_o^2)^2]^{1/2}$.

Table 2. Selected Bond Distances (Å) for $Na_{1.4}Nb_3Te_{4.9}O_{18}$ and $NaNb_3Te_4O_{16}$

$Na_{1.4}Nb_3Te_{4.9}O_{18}$		$NaNb_3Te_4O_{16}$	
Nb(1)−O(1) × 2	2.006(4)	Nb(1)−O(1) × 2	1.988(4)
Nb(1)−O(2) × 2	1.999(4)	Nb(1)−O(2) × 2	1.980(4)
Nb(1)−O(3) × 2	1.9569(18)	Nb(1)−O(3) × 2	1.957(2)
Nb(2)−O(4)	2.067(4)	Nb(2)−O(2)	1.837(4)
Nb(2)−O(5)	1.9525(19)	Nb(2)−O(4)	2.020(4)
Nb(2)−O(6)	1.984(4)	Nb(2)−O(5)	2.013(4)
Nb(2)−O(7)	1.9014(14)	Nb(2)−O(6)	1.971(2)
Nb(2)−O(8)	2.024(4)	Nb(2)−O(7)	2.124(4)
Nb(2)−O(9)	1.967(2)	Nb(2)−O(8)	1.961(2)
Te(1)−O(2) × 2	1.936(5)	Te(1)−O(4)	1.890(4)
Te(1)−O(10)	2.235(7)	Te(1)−O(4)	1.890(5)
Te(1)−O(12)	2.098(6)	Te(1)−O(9)	2.022(6)
Te(2)−O(1) × 2	1.930(4)	Te(1)−O(10)	2.176(7)
Te(2)−O(10)	1.881(6)	Te(2)−O(5)	1.910(4)
Te(3)−O(6) × 2	1.946(4)	Te(2)−O(5)	1.910(5)
Te(3)−O(13)	1.831(6)	Te(2)−O(11)	1.842(7)
Te(4)−O(4) × 2	1.894(4)	Te(3)−O(1) × 2	1.909(5)
Te(4)−O(11)	2.427(7)	Te(3)−O(10)	1.810(7)
Te(4)−O(12)	1.955(6)	Te(4)−O(7) × 2	1.880(5)
Te(5)−O(8) × 2	1.919(5)	Te(4)−O(9)	2.006(6)
Te(5)−O(11)	1.840(7)	Te(4)−O(11)	2.417(6)

Raman spectra were recorded at room temperature on a Digilab FTS 7000 spectrometer equipped with a germanium detector with the powder sample placed in separate capillary tubes. Excitation was provided by a Nd:YAG laser at a wavelength of 1064 nm, and the output laser power was 500 mW. The spectral resolution was about 4 cm^{-1}, and 200 scans were collected for each sample.

UV−Vis Diffuse Reflectance Spectroscopy. UV−vis diffuse reflectance data for $Na_{1.4}Nb_3Te_{4.9}O_{18}$ and $NaNb_3Te_4O_{16}$ were collected with a Varian Cary 500 scan UV−vis−NIR spectrophotometer over the spectral range 200−1500 nm at room temperature. Poly(tetrafluoroethylene) was used as a reference material. Reflectance spectra were converted to absorbance with the Kubelka−Munk values.[40]

Thermogravimetric Analysis. Thermogravimetric analyses were carried out on a TGA 2950 thermogravimetric analyzer (TA Instruments). The samples were contained within platinum crucibles and heated at a rate of 10 °C min^{-1} from room temperature to 1000 °C in static air.

Dielectric Characterization. Dielectric constant (κ) measurements were performed using a HP4192A impedance analyzer operating at 1 MHz. Polycrystalline $Na_{1.4}Nb_3Te_{4.9}O_{18}$ and $NaNb_3Te_4O_{16}$ were pressed into 1.2 cm diameter and 0.15 cm thick pellets and sintered at 700 °C for 24 h. The pellets had a density 90% theoretical. Conducting silver paste was applied to the pellet surfaces as electrodes and cured at 400 °C. The temperature dependence of the dielectric constant (TCK) was measured, between −20 and 100 °C, by placing the pellets in a Linkam THMSE600 hot stage.

Results

Structures. The mixed-metal oxide, $Na_{1.4}Nb_3Te_{4.9}O_{18}$, exhibits a three-dimensional structure consisting of chains of corner-shared NbO_6 octahedra connected by asymmetric TeO_3 and TeO_4 polyhedra. The two unique Nb^{5+} cations are in octahedral coordination environments bonded to six oxygen atoms, with Nb−O bond distances ranging from 1.9014(14) to 2.067(4) Å. The Nb(1) cation has an almost regular octahedral coordination environment, whereas the Nb(2) cation is distorted toward a corner of its oxide octahedron (local C_4 direction), creating an asymmetric Nb^{5+} coordination environment. We will be discussing all of the cationic distortions in more detail later in the paper. Three of the five unique Te^{4+} cations are in distorted trigonal pyramidal environments, i.e., TeO_3 polyhedra, whereas two Te^{4+} cations exhibit seesaw geometry, i.e., TeO_4 polyhedra. These asymmetric coordination environments can be attributed to the nonbonded electron pair on the Te^{4+} cation. The Te−O bond distances range from 1.831(6) to 2.427(7) Å. The Na^+ cations are in 8-fold coordination environments, with Na−O contacts ranging from 2.405(5) to 2.839(6) Å. Bond valence calculations,[41,42] weighted to reflect occupancies, resulted in values 0.93, 3.57−3.86, and 4.89−5.00 for Na^+, Te^{4+}, and Nb^{5+}, respectively for $Na_{1.4}Nb_3Te_{4.9}O_{18}$.

The structural backbone of $Na_{1.4}Nb_3Te_{4.9}O_{18}$ may be considered as two sets of corner-shared NbO_6 octahedral chains (see Figure 1a,b). The "first" chain consists of one row of corner-shared NbO_6 octahedra that are linked by TeO_3 and TeO_4 polyhedra (see Figure 1a), whereas the "second" chain consists of two rows of corner-shared NbO_6 octahedra that are linked by TeO_3 groups (see Figure 1b). Each of these chains of octahedra runs parallel to the [010] direction. The "first" and "second" chains are linked by the TeO_3 and TeO_4 groups, along the [100] and [010] directions resulting in the three-dimensional topology (see Figure 1c). The Te^{4+} cation that connects the two chains is partially occupied with a refined occupancy of approximately 0.90. The Na^+ cations reside in the spaces between the two chains.

The second reported material, $NaNb_3Te_4O_{16}$, also exhibits a three-dimensional crystal structure consisting of corner-linked NbO_6 octahedra that are connected to asymmetric TeO_3 and TeO_4 groups. The two unique Nb^{5+} cations are in octahedral coordination environments bonded to six oxygen atoms, with Nb−O bond distances ranging from 1.837(4) to 2.124(4) Å. Similar to $Na_{1.4}Nb_3Te_{4.9}O_{18}$, the Nb(1) cation has an almost regular octahedral environment, whereas the Nb(2) cation is distorted, toward a corner of its oxide octahedron (local C_4 direction), creating an asymmetric Nb^{5+} coordination environment. Two of the four unique Te^{4+} cations are in distorted trigonal pyramidal environments, i.e.,

(40) Kubelka, P.; Munk, F. *Z. Tech. Phys.* **1931**, *12*, 593.

(41) Brown, I. D.; Altermatt, D. *Acta Crystallogr.* **1985**, *B41*, 244.

(42) Brese, N. E.; O'Keeffe, M. *Acta Crystallogr.* **1991**, *B47*, 192.

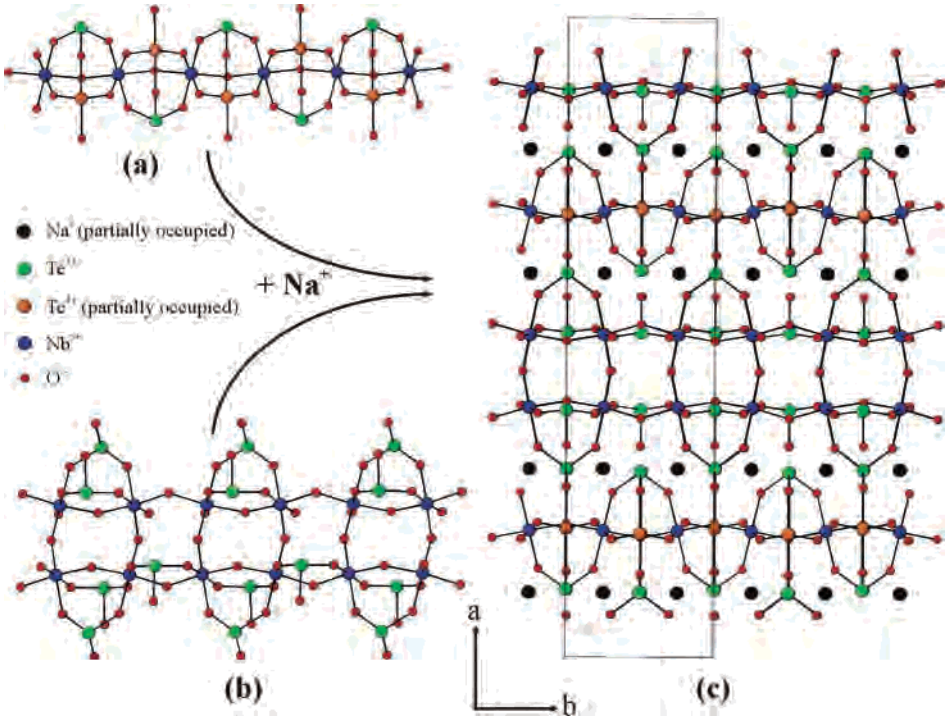

Figure 1. Ball-and-stick diagram of $Na_{1.4}Nb_3Te_{4.9}O_{18}$ in the *ab*-plane. Note the spaces in the structure where the Na^+ cation and lone pair on the Te^{4+} cation reside.

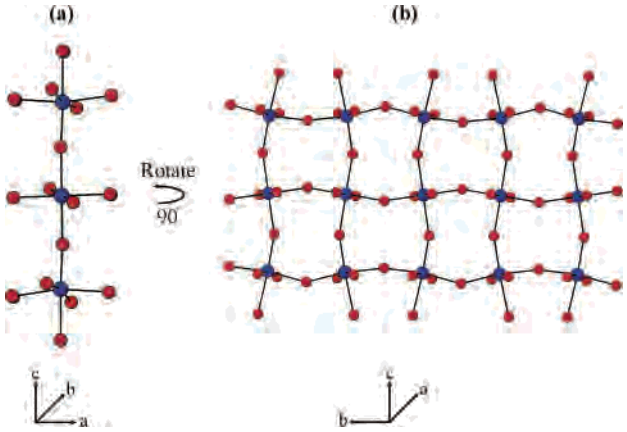

Figure 2. Ball-and-stick diagram of the NbO_6 octahedra in $NaNb_3Te_4O_{16}$.

TeO_3 polyhedra, whereas the other two Te^{4+} cations exhibit seesaw geometry, i.e., TeO_4 polyhedra. As with the Te^{4+} cations in $Na_{1.4}Nb_3Te_{4.9}O_{18}$, the asymmetric environments may be attributable to the nonbonded electron pair. The Te−O bond distances range from 1.810(7) to 2.417(6) Å. The Na^+ cations are in 8-fold coordination environments with Na−O contacts ranging from 2.479(4) to 2.831(5) Å. Bond valence calculations[41,42] on $NaNb_3Te_4O_{16}$ resulted in values 0.92, 3.83−4.00, and 5.01−5.05 for Na^+, Te^{4+}, and Nb^{5+}, respectively.

Similar to $Na_{1.4}Nb_3Te_{4.9}O_{18}$, the structural backbone of $NaNb_3Te_4O_{16}$ may also be considered as an infinite chain of corner-shared NbO_6 octahedra. The chain consists of three corner-shared NbO_6 octahedra running along the [001] direction. These octahedra are infinite, through additional corner-sharing, in the [010] direction (see Figure 2a,b). The TeO_3 and TeO_4 groups serve to link these NbO_6 octahedra. The $Te(1)O_4$, $Te(2)O_3$, and $Te(3)O_3$ polyehdra connect the

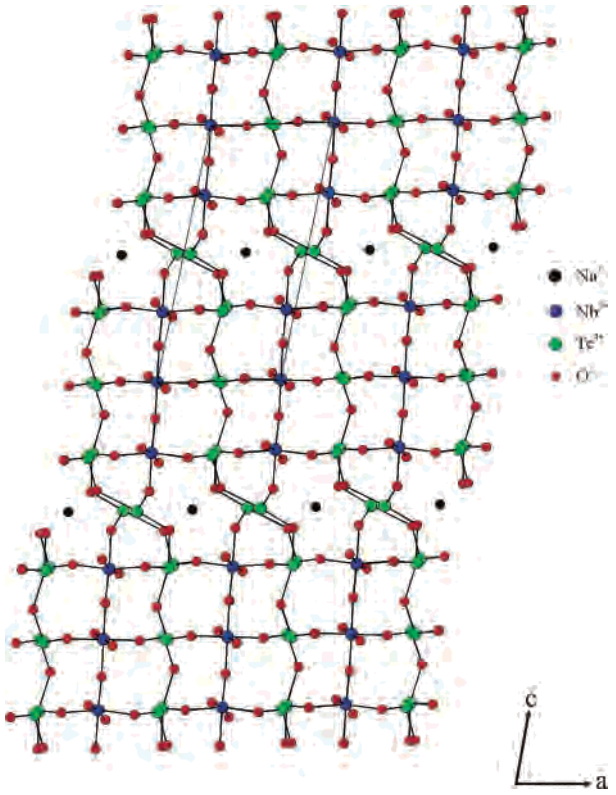

Figure 3. Ball-and-stick representation of $NaNb_3Te_4O_{16}$ in the *ac*-plane. Note that the NbO_6 octahedra are linked along the [100] and [001] directions by TeO_3 and TeO_4 groups.

octahedra along the [100] direction, whereas the $Te(4)O_4$ polyhedra links the octahedra along the [001] direction. Figure 3 gives a ball-and-stick representation of all these linkages. The Na^+ cations reside in the spaces between the NbO_6 octahedra.

Table 3. Infrared and Raman Vibrations (cm^{-1}) for $Na_{1.4}Nb_3Te_{4.9}O_{18}$ and $NaNb_3Te_4O_{16}$

$Na_{1.4}Nb_3Te_{4.9}O_{18}$			$NaNb_3Te_4O_{16}$		
Nb−O	Te−O	Nb−O−Te	Nb−O	Te−O	Nb−O−Te
		IR (cm^{-1})			
941	808	651	939	806	657
900	740	617	896	740	617
530	669		526	719	
	472			700	
	437			680	
				667	
				472	
				447	
		Raman (cm^{-1})			
926	779	636	933	783	648
875	748	613	844	744	605
547	671		547	671	
	462			478	
	443			439	
	393			420	
				389	

Infrared and Raman Spectroscopy. The infrared and Raman spectra of $Na_{1.4}Nb_3Te_{4.9}O_{18}$ and $NaNb_3Te_4O_{16}$ revealed Nb−O, Te−O, and Nb−O−Te vibrations. Nb−O and Te−O vibrations are observed between 900 and 940 and 660 and 800 cm^{-1}, respectively in both the IR and Raman. Multiple bands, occurring between 600 and 660 cm^{-1}, are attributable to Nb−O−Te vibrations. The infrared and Raman vibrations and assignments for $Na_{1.4}Nb_3Te_{4.9}O_{18}$ and $NaNb_3Te_4O_{16}$ are listed in Table 3. The assignments are consistent with those previously reported.[43−46]

UV−Vis Diffuse Reflectance Spectroscopy. The UV−Vis diffuse reflectance spectra for $Na_{1.4}Nb_3Te_{4.9}O_{18}$ and $NaNb_3Te_4O_{16}$ are deposited in the Supporting Information. Both of the compounds are white, and the spectra indicate that they are transparent. Absorption (K/S) data were calculated from the following Kubelka−Munk function:

$$F(R) = \frac{(1-R)^2}{2R} = \frac{K}{S}$$

Here R represents the reflectance, K the absorption, and S the scattering. In a K/S vs E (eV) plot, extrapolating the linear part of the rising curve to zero provides the onset of absorption at 3.2 and 3.6 eV for $Na_{1.4}Nb_3Te_{4.9}O_{18}$ and $NaNb_3Te_4O_{16}$, respectively. The overall band gap for each material may be attributable to the degree of Nb (4d) orbitals that are engaged in the conduction bands as well as the distortions arising from TeO_3 and TeO_4 polyhedra.

Thermogravimetric Analysis. The thermal behavior of $Na_{1.4}Nb_3Te_{4.9}O_{18}$ and $NaNb_3Te_4O_{16}$ was investigated using thermogravimetric analysis. Both materials are not stable at higher temperatures. In each case, single-step decompositions occur indicating volatilization above 740 °C for $Na_{1.4}Nb_3Te_{4.9}O_{18}$ and 730 °C for $NaNb_3Te_4O_{16}$. Powder XRD measurements on the calcined materials revealed a mixture of Nb_2O_5, $NaNb_{13}O_{33}$,[47] $Te_3Nb_2O_{11}$,[27] and unknown amorphous materials for $Na_{1.4}Nb_3Te_{4.9}O_{18}$ and Nb_2O_5, $Na_2Nb_4O_{11}$,[48] and unknown amorphous materials for $NaNb_3Te_4O_{16}$.

Table 4. Dielectric Constant (κ), Quality Factor (Q), and Temperature Coefficient of the Dielectric Constant (TCK) for $Na_{1.4}Nb_3Te_{4.9}O_{18}$ and $NaNb_3Te_4O_{16}$ at 1 MHz and 20 °C[a]

	k	Q	TCK (ppm/°C)
$Na_{1.4}Nb_3Te_{4.9}O_{18}$	44.16	66.7	382
$NaNb_3Te_4O_{16}$	39.96	>100	1196

[a] $Q = 1/\tan\delta$; TCK $= [(\kappa_{100} - \kappa_{-20})/\kappa_{40}]/120$.

Dielectric Measurements. The dielectric constants at 1 MHz are $\kappa = 44.16$ and 39.96 for $Na_{1.4}Nb_3Te_{4.9}O_{18}$ and $NaNb_3Te_4O_{16}$, respectively. With the temperature dependence of the dielectric constant (TCK), the values for $Na_{1.4}Nb_3Te_{4.9}O_{18}$ are 382 and $NaNb_3Te_4O_{16}$ are 1196 ppm/°C (see Table 4). Additional measurements including variable frequency measurements (at 10 kHz, 100 kHz, and 1 MHz) are underway to ascertain the origin of this dielectric behavior.

Discussion

Although both $Na_{1.4}Nb_3Te_{4.9}O_{18}$ and $NaNb_3Te_4O_{16}$ crystallize in centrosymmetric space groups, the materials contain cations in distorted coordination environments, i.e., Nb^{5+} and Te^{4+}. One of our motivations for investigating materials containing both d^0 transition metals and lone-pair cations is to better understand these distortions and coordination environments. Both of the reported compounds contain NbO_6 and TeO_x ($x = 3$ or 4) polyhedra. Two unique NbO_6 octahedra are observed in both materials. Interestingly, only one of the two unique Nb^{5+} cations, in each compound, is in an asymmetric coordination environment. A ball-and-stick representation of the Nb^{5+} coordination environments in both materials is shown in Figure 4. As seen, Nb(1) is in the center of its oxygen octahedron, i.e., undistorted. We have described a manner in which the extent of the distortion can be quantified.[35] Using this methodology, we determined that the extent of the distortion, Δ_d, for Nb(1) in both $Na_{1.4}Nb_3Te_{4.9}O_{18}$ and $NaNb_3Te_4O_{16}$ is 0.00. A different situation is observed for Nb(2). In both materials, the Nb(2) cation is distorted toward a corner of its octahedron, i.e., a C_4 distortion. These C_4-Nb(2) displacements result in four normal, one short, and one long Nb−O bonds (see Figure 4). The Δ_d's for the C_4-Nb(2) cations are 0.22 and 0.31 for $Na_{1.4}Nb_3Te_{4.9}O_{18}$ and $NaNb_3Te_4O_{16}$, respectively. The direction of the distortion is consistent for what is commonly observed with Nb^{5+}; however, the magnitude is smaller than the average value for Nb^{5+} (0.62). Table 5 summarizes the direction and magnitude of the Nb^{5+} distortions. With the distorted Nb(2) cation, we note that the distortion is away from the oxide that bridges to a Te^{4+} cation. This C_4-Nb^{5+} distortion may be considered as a primary distortion, attributable to electronic, i.e., SOJT effects. The secondary

(43) Bart, J. C. J.; Petrini, G. *Z. Anorg. Allg. Chem.* **1980**, *466*, 81.
(44) Arnaudov, M.; Dimitrov, V.; Dimitriev, Y.; Markova, L. *Mater. Res. Bull.* **1982**, *17*, 1121.
(45) Judd, D. A.; Chen, Q.; Campana, C. F. *J. Am. Chem. Soc.* **1997**, *119*, 5461.
(46) Kim, G.-S.; Zeng, H.; VanDerveer, D.; Hill, C. L. *Angew. Chem., Int. Ed. Engl.* **1999**, *38*, 3205.
(47) Anderson, S. *Acta Chem. Scand.* **1965**, *19*, 557.
(48) Jahnberg, L. *J. Solid State Chem.* **1970**, *1*, 454.

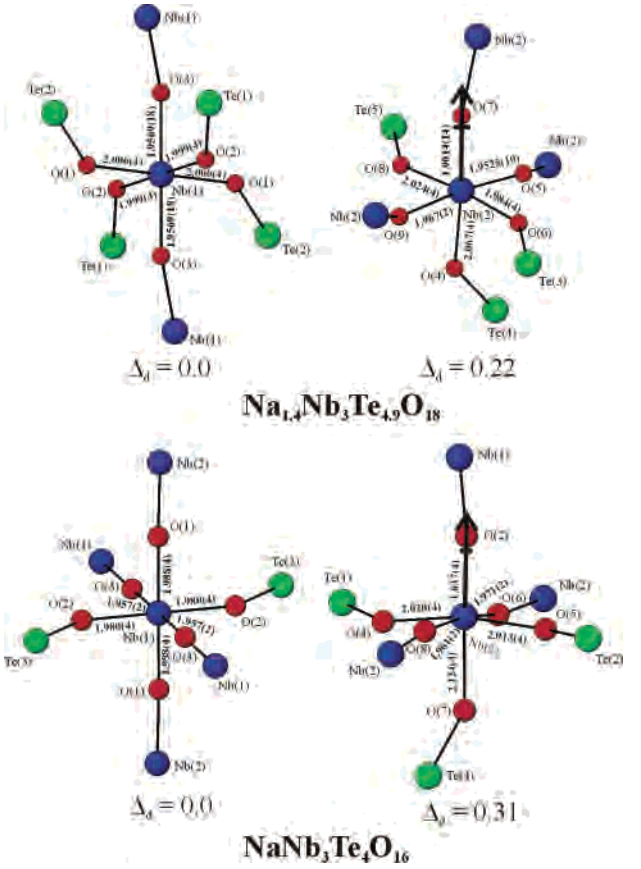

Figure 4. Ball-and-stick diagram of the local coordination of the Nb^{5+} cation in $Na_{1.4}Nb_3Te_{4.9}O_{18}$ and $NaNb_3Te_4O_{16}$. In both materials Nb(1) is undistorted, whereas Nb(2) undergoes an out-of-center displacement toward a corner, i.e., a C_4 distortion.

Table 5. Direction and Magnitude of the Nb^{5+} Cation Distortion in $Na_{1.4}Nb_3Te_{4.9}O_{18}$ and $NaNb_3Te_4O_{16}$

compd	distortion	magnitude
$Na_{1.4}Nb_3Te_{4.9}O_{18}$	nd[a]	0.00
	C_4	0.22
$NaNb_3Te_4O_{16}$	nd[a]	0.00
	C_4	0.31

[a] nd = no distortion.

distortion involves the interaction between the NbO_6 octahedra and TeO_x ($x = 3$ or 4) polyhedra. We have previously discussed that, in oxides containing octahedrally coordinated d^0 transition metals linked to lone-pair polyhedra, the displacement of the d^0 transition metal will be away from the oxide bridging to the lone-pair cation. We attribute this to the structural rigidity, or predistorted nature, of the lone-pair polyhedra. If the d^0 transition metal were to distort toward the lone-pair cation, a compensating distortion in the lone-pair polyhedron must occur. This is extremely unlikely, since the lone-pair polyhedra is already in an extremely distorted environment and any additional distortion would be unfavorable. Thus, the primary distortion is supported and reinforced by the secondary distortion, as the d^0 transition metal displaces away from the lone-pair cation.

The direction and magnitude of the distortions in the NbO_6, TeO_4, and TeO_3 polyhedra may also be quantified by determining the local dipole moments. This approach has been described earlier.[49,50] In both instances metal oxide−fluoride octahedra were investigated. The method uses a bond-valence approach to calculate the direction and magnitude of the local dipole moments. We have extended this approach to include lone-pair polyhedra. With the lone-pair polyhedra, the lone pair is given a charge of −2 and localized 1.25 Å from the Te^{4+} cation. This Te^{4+}−lone-pair distance is based on earlier work by Galy et al.[51] Using this methodology, the dipole moment for the TeO_4 and TeO_3 polyhedra is in the opposite direction of the lone pair. We have calculated the dipole moment of the NbO_6, TeO_4, and TeO_3 polyhedra in $Na_{1.4}Nb_3Te_{4.9}O_{18}$ and $NaNb_3Te_4O_{16}$. For comparison, we have also calculated the dipole moment for similar polyhedra in other Nb^{5+}−Te^{4+}−oxides as well as TeO_2 (see Table 6). As seen in Table 6, the magnitude of the NbO_6 dipole moment in $Na_{1.4}Nb_3Te_{4.9}O_{18}$ and $NaNb_3Te_4O_{16}$ is somewhat smaller than what is usually observed for C_4-Nb^{5+} distortions. Interestingly with Te^{4+}, there is only a small difference in the magnitude of the dipole moment comparing TeO_4 with TeO_3. In fact an examination of 24 examples of TeO_4 and 31 of TeO_3 polyhedra resulted in average dipole moments of 8.6 and 8.7 D, respectively. We are in the process of examining all Te^{4+} oxides that contain TeO_3, TeO_4, or TeO_5 groups to better understand the asymmetric polar environment.[52]

Table 6. Calculation of Dipole Moments for NbO_6, TeO_4, and TeO_3 Polyhedra. D = Debyes

compd	distortn symm-species	dipole moment (D)
$Na_{1.4}Nb_3Te_{4.9}O_{18}$	nd[a]-Nb(1)O_6	0.0
	C_4-Nb(2)O_6	2.3
	Te(1)O_4	5.2
	Te(2)O_3	7.8
	Te(3)O_3	7.8
	Te(4)O_4	8.0
	Te(5)O_3	8.7
$NaNb_3Te_4O_{16}$	nd[a]-Nb(1)O_6	0.0
	C_4-Nb(2)O_6	3.1
	Te(1)O_4	8.5
	Te(2)O_3	8.8
	Te(3)O_3	8.8
	Te(4)O_4	7.4
$Nb_2Te_4O_{13}$[29]	C_4-Nb(1)O_6	2.2
	C_4-Nb(2)O_6	3.1
	C_4-Nb(3)O_6	3.4
	C_4 - Nb(4)O_6	3.2
	TeO_4 × 4 (av)	8.4
	TeO_3 × 3 (av)	8.2
$Te_4Nb_3O_{15}$·Cl[31]	C_4-Nb(1)O_6	3.5
	C_4-Nb(2)O_6	4.3
	C_4-Nb(3)O_6	4.6
	TeO_3 × 4 (av)	8.8
TeO_2[53]	Te(1)O_4	7.3
TeO_4 polyhedra	TeO_4(av)	8.6
24 examples[b]	TeO_4(range)	5.2−11.1
TeO_3 polyhedra	TeO_3(av)	8.7
31 examples[b]	TeO_3(range)	6.6−10.5

[a] nd = no distortion. [b] In Supporting Information.

Acknowledgment. We thank the Robert A. Welch Foundation for support. This work was also supported by

(49) Maggard, P. A.; Nault, T. S.; Stern, C. L.; Poeppelmeier, K. R. *J. Solid State Chem.* **2003**, *175*, 25.
(50) Izumi, H. K.; Kirsch, J. E.; Stern, C. L.; Poeppelmeier, K. R. *Inorg. Chem.* **2005**, *44*, 884.
(51) Galy, J.; Meunier, G. *J. Solid State Chem.* **1975**, *13*, 142.
(52) Ok, K. M.; Halasyamani, P. S. **2005**, in press.
(53) Thomas, P. A. *J. Phys. C. Solid State* **1988**, *21*, 4611.

the NSF-Career Program through Grant DMR-0092054. P.S.H. is a Beckman Young Investigator. We also acknowledge Jason Locklin and Prof. Rigoberto Advincula for assistance in obtaining the Raman spectra.

Supporting Information Available: X-ray crystallographic files for $Na_{1.4}Nb_3Te_{4.9}O_{18}$ and $NaNb_3Te_4O_{16}$ in CIF format, ORTEP diagrams, calculated and observed X-ray diffraction patterns for $Na_{1.4}Nb_3Te_{4.9}O_{18}$ and $NaNb_3Te_4O_{16}$, and dipole moment calculations. This material is available free of charge via the Internet at http://pubs.acs.org.

IC050256B